Journal of Materials Chemistry A

REVIEW

View Article Online
View Journal | View Issue

Cite this: J. Mater. Chem. A, 2023, 11, 3281

Photoelectrocatalytic organic synthesis: a versatile method for the green production of building-block chemicals

Si-Yang Li, [abc] Ke-Fu Huang, [c] Zhi-Yong Tang [ac] and Jing-Hao Wang *[ac]

Received 4th December 2022
Accepted 13th January 2023

DOI: 10.1039/d2ta09430d

rsc.li/materials-a

The rising energy crisis and environmental problems are urging the development of more sustainable organic synthetic methods. Photoelectrocatalytic organic synthesis (PECOS) is emerging as an attractive strategy because it utilizes solar power to drive the organic synthesis and can greatly reduce the dependency on fossil fuels. Recently, a variety of organic reactions have been successfully realized using this strategy by rationally designing the photoelectrode and carefully tuning the reaction conditions. In this review, we introduce and categorize the recent advances in PECOS based on their specific reaction types, ranging from photoanode-mediated alcohol oxidation, C–H functionalization, furan oxidation, and sulfide oxidation, to (photo) cathode-mediated *in situ* H_2O_2 generation, cofactor regeneration, and the functionalization of aryl halides. The material of the photoelectrode, the reaction conditions of PECOS, and the proposed mechanism will be highlighted during the introduction of each example. Finally, we conclude by providing some perspectives on the future direction of PECOS.

1. Introduction

As a sustainable, cost-free, environment-friendly energy, solar power has been continuously gaining the scientific community's attention.[1,2] Fixing solar energy in value-added compounds, like fuels and building-block chemicals, is a promising way to realize the storage of solar energy and has received considerable attention from the chemical community.[3–6] Developing green and efficient methods of converting solar energy into chemical energy is becoming the future trend of energy and synthetic chemistry.

Inheriting the advantages of photocatalysis and electrocatalysis, photoelectrocatalysis is a potential candidate for the green and efficient conversion of solar power. A typical setup for photoelectrocatalysis consists of a semiconductor photoelectrode and a counter electrode. Upon light irradiation, an electron and hole are separated at the photoelectrode. One of them migrates to the surface of the photoelectrode and motivates the redox reactions; with the help of an external circuit, another would transfer to the counter electrode (in the case of he photoanode) or be neutralized by the electron transported from the counter electrode (in the case of the photocathode).[7] Compared with photocatalysis, the separation efficiency of photogenerated carriers could be tuned by the external potential in photoelectrocatalysis, enabling the careful control of reaction selectivity.[8,9] Besides, the existence of an external circuit allows the reduction and oxidation half reactions to take place in different electrodes, making it possible to conduct the reductive and oxidative synthesis in a spatially separated manner.[10] The spatial separation of reduction and oxidation half reactions can prevent the undesired side reactions of the products and overcome the product separation problems in photo-redox organic synthesis.[11,12] In the meantime, the introduction of light energy reduces the applied bias so that photoelectrocatalysis could be carried out in a more energy-saving manner than electrocatalysis. It should be noticed that there is another kind of organic synthesis which is conducted using the combination of inert electrodes and photocatalyst: upon light irradiation, the photocatalyst were first transformed into their excited state, which then participate in the redox reaction of the organic substrates; with the help of inert electrodes, the photocatalysts are finally regenerated. In fact, this kind of catalysis could be classified as "electrophotocatalysis" and König, Wu, and Lambert *et al.* have already presented some excellent studies on this topic.[13–15]

Since Fujishima and Honda reported the feasibility of photoelectrocatalytic water splitting,[16] for the first time, much effort has been put into the development of photoelectrocatalysis. Nowadays, the application of photoelectrochemical cells (PECs) is no longer limited to the decomposition of water. The capability of PECs in fuel production,[17–23] carbon dioxide reduction,[24–29] and biomass conversion[30–36] has been widely

[a]Chinese Academy of Science (CAS) Key Laboratory of Nanosystem and Hierarchy Fabrication, CAS Center for Excellence in Nanoscience, National Center for Nanoscience and Technology, Beijing 100190, P. R. China

[b]Sino-Danish College, University of Chinese Academy of Sciences, Beijing 100049, P. R. China

[c]University of Chinese Academy of Sciences, Beijing 100049, P. R. China

investigated. However, the research on photoelectrocatalytic organic synthesis (PECOS) is still in an early stage.

In the past decade, many attempts on promoting the development of PECOS have been made. The photoelectrode material, the reaction type, and the substrate scope of PECOS have been greatly diversified. Now, PECs equipped with a classical metal oxide photoanode can do much more than oxidizing simple alcohols.[37] More complex oxidations such as the functionalization of a C–H bond and the selective oxidation of polyhydric alcohol, furan, and sulfide can also be realized. Besides, by properly introducing enzymes or heterogenous catalysts, the place where redox reactions take place is no longer limited to the photoanode, which makes the cathode-mediated PECOS possible. Moreover, the successful application of photocathodes in PECs further broadens the reaction types of PECOS. This progress shows the compatibility of PECs with organic synthesis.

In this article, we provide a concise review of the recent development of PECOS. Based on the exact electrode which mediates the organic synthesis, we classify the literature into two main categories: photoanode-mediated organic synthesis and (photo) cathode-mediated organic synthesis. Each category is further divided into subcategories according to the specific reaction types. Finally, we offer some perspectives on the future direction of PECOS.

2. Photoanode-mediated organic synthesis

The most common type of PECOS is carried out in a photoanode-mediated manner, in which photogenerated holes directly or indirectly oxidize the organic substrates. In direct oxidation, the organic substrates are oxidized on the surface of a photoanode (Fig. 1A). Generally speaking, the careful control of the reaction selectivity is relatively difficult to obtain in direct oxidation because of the high reactivity of photogenerated holes.[38–40] In indirect oxidation, however, the photogenerated holes first oxidize the redox mediator to form a reactive intermediate, which then oxidizes the organic substrates and return to its original state (Fig. 1B). With these two kinds of reaction pathways, the photoanode-mediated organic synthesis reported thus far exhibits diverse reaction types, which are roughly classified into alcohol oxidation, C–H functionalization, and the oxidation of other organic compounds.

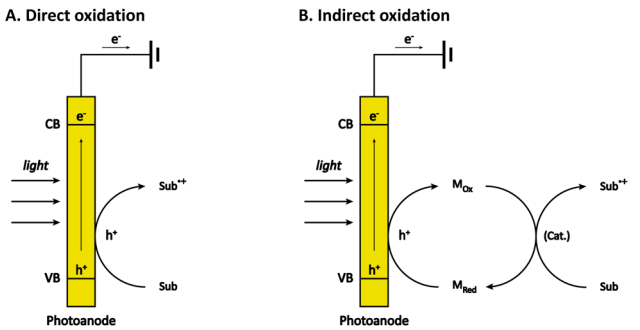

Fig. 1 Schematics for direct and indirect oxidation on a photoanode.

2.1 Alcohol oxidation

According to the structural complexity of alcohol molecules, we divide the alcohol oxidation that happens in PECs into the oxidation of simple alcohols and the oxidation of polyhydric alcohols. Since simple alcohols have only one hydroxyl group, their oxidation has no regioselectivity problem. In contrast, the regioselectivity must be taken into account if one wants to achieve the selective oxidation of polyhydric alcohols with hydroxyl groups within different environments.

2.1.1 Oxidation of simple alcohols. The history of PEC-mediated simple alcohol oxidation dates back to 1999, when Meyer's group reported the dehydrogenation of 2-propanol into acetone on a dye-sensitized TiO_2 photoanode,[41] which preliminarily exhibited the feasibility of PECOS. After that, many dye-sensitized photoelectrochemical cells (DSPECs) have been developed for the oxidation of simple alcohols.[42–48]

In 2020, Meyer and co-workers introduced organic photosensitizers to the surface of a SnO_2/TiO_2 photoanode.[46] The phosphonate-derivatized carbazole and boron dipyrromethene ($BODIPY(CBZ)_2PO_3H_2$) chromophore (**3**) has a high molar extinction coefficient and good visible light response. Together with a ruthenium-based catalyst (**4**), the photoanode could sustain the oxidation of benzyl alcohol (**1a**) in a pH 4.5 acetic buffer under visible light irradiation. At an applied bias of 0.2 V *vs.* Ag/AgCl, the density of photocurrent was maintained at around 35 μA cm^{-2}. The low current level may be caused by the back electron transfer after electron injection.[49]

Even though being frequently used,[41–46,50] ruthenium-based dye molecules are not the only choice for the photosensitizer used in a DSPEC. The noble metal ruthenium could be replaced by earth-abundant elements as well.[51,52] For example, Nikoloudakis *et al.* presented efficient and selective conversion from para-substituted phenyl alcohols (**1a–1c**) into the corresponding aldehydes (**2a–2c**) with a zinc porphyrin (ZnP) sensitizer (**5**).[47] The photosensitizer was anchored on the surface of a TiO_2 photoanode by a robust hydroxamic group and hence was able to work both in aqueous solutions and organic solvents. ZnP was also covalently linked with 2,2,6,6-tetramethyl-1-piperidine *N*-oxyl (TEMPO), which served as the catalyst for alcohol oxidation. Upon light illumination, the holes generated by ZnP efficiently transferred to TEMPO, thus realizing the selective production of *para*-methoxy benzaldehyde with an average photocurrent density of 200 μA cm^{-2} at 0 V *vs.* SCE in a pH 8.0 borate buffer.

Recently, Reisner's group established a DSPEC where both the dye molecule and alcohol oxidation catalyst were metal-free.[48] The photoanode was prepared by co-immobilizing silatrane-functionalized TEMPO (STEMPO, **6**) and diketopyrrolopyrrole-based dye (DPP-CA, **7**) on mesoporous TiO_2 ($mTiO_2$). Under the irradiation of ultraviolet-filtered simulated solar light, 4-methylbenzylalcohol (**1d**) can be selectively oxidized to its aldehyde form on this photoanode with a photocurrent density of around 90 μA cm^{-2} at +0.4 V *vs.* RHE

in pH 8.0 sodium borate buffer. The author also coupled the photoanode with a CO_2-reducing cathode. The as-constructed PEC could achieve a bias-free, simultaneous alcohol oxidation and CO_2 reduction with a photocurrent density up to 30 μA cm^{-2}.

The oxidation of simple alcohol can also be realized in PECs without dye molecules. Earlier in 2017, the oxidation of 1-phenylethanol derivatives on a $BiVO_4/WO_3$ photoanode was reported by Sayama's group.[53] 1-phenylethanol derivatives (**1e–1i**) were directly oxidized by the photogenerated holes at the surface of the photoanode. The applied potential required for oxidation in this system (approximately +0.7 V *vs.* SHE) was much lower than that in an electrocatalytic system taking Pt as the anode (>1.9 V *vs.* SHE). Meanwhile, the para-substituent effect observed in an electrocatalytic system was negligible in this system, suggesting that the external bias did not influence the oxidation ability of photogenerated holes. Under visible light irradiation (>420 nm), 1-phenylethanol can be oxidized with excellent yield (97%) and faradaic efficiency (>99%).

In the same year, Duan and co-workers developed a TiO_2/C composite photoanode and tested its catalytic performance on the oxidation of benzyl alcohol derivatives (**1a**, **1d**, **1j**, & **1k**).[54] The photoanode was prepared through a three-step method: first, TiO_2 nanowire arrays, with an average diameter of around 200 nm, were hydrothermally grown on a fluorine-doped tin oxide (FTO) substrate; then, polypyrrole was coated on the surface of TiO_2 *via* a photo-assisted deposition method; finally, calcination in a N_2 atmosphere finally led to the formation of a graphite coating layer. The existence of a graphite layer maximized the separation efficiency of photogenerated carriers

Table 1 Photoanode-mediated benzyl alcohol oxidation

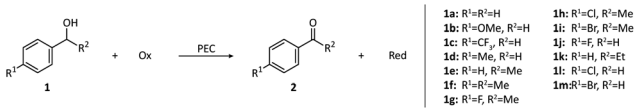

Substrate	Photoanode	Conditions	Ox/red	Performance	Ref.
1a	SnO_2|TiO_2|-**3,4**	0.2 V *vs.* Ag/AgCl, 100 mW cm^{-2} visible light, 0.4 M $LiClO_4$ pH 4.5 acetic buffer	H^+/H_2	$J \approx 35$ μA cm^{-2}	46
1a	TiO_2|**5**	0 V *vs.* SCE, 100 mW cm^{-2} visible light, 0.1 M $NaClO_4$ pH 8.0 borate buffer	H^+/H_2	$J \approx 0.19$ mA cm^{-2}	47
1b				$J \approx 0.20$ mA cm^{-2}	
1c				$J \approx 0.50$ mA cm^{-2}	
1d	mTiO_2|**6,7**	Bias-free, 100 mW cm^{-2} visible light, pH 8.0 borate buffer	CO_2/formate	$J \approx 30$ μA cm^{-2}	48
1e	$BiVO_4/WO_3$	0.2 mA cm^{-2}, 100 mW cm^{-2} visible light, 0.1 M Bu_4NBF_4, MeCN	NA	Yield 97%	53
1f				Yield 63%	
1g				Yield 89%	
1h				Yield 92%	
1i				Yield 91%	
1a	TiO_2/C	0.6 V *vs.* SCE, 120 mW cm^{-2} Xe lamp, 0.5 M Na_2SO_4	H^+/H_2	144 μmol h^{-1}	54
1d				180 μmol h^{-1}	
1j				161 μmol h^{-1}	
1k				45 μmol h^{-1}	
1a	G@U-LDH@BVO	1.2 V *vs.* RHE, 100 mW cm^{-2} visible light, 8 mL pH 7.0 PBS solution, 2 mL MeCN	H^+/H_2	150 μmol h^{-1}	55
1d				188 μmol h^{-1}	
1j				144 μmol h^{-1}	
1l				125 μmol h^{-1}	
1m				151 μmol h^{-1}	

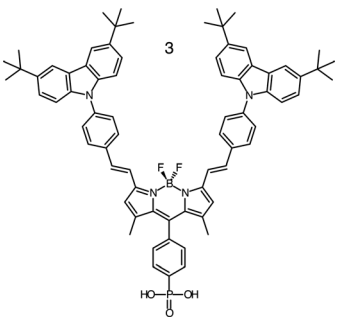

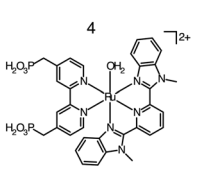

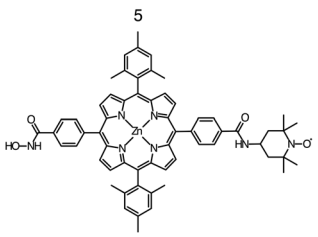

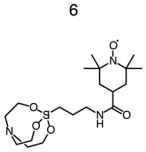

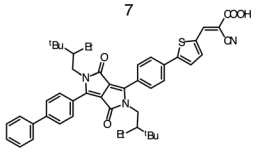

and accelerated the oxidation of H_2O to generate $O_2^{\cdot-}$, which plays an important role in alcohol oxidation. With the help of light and external bias, the TiO_2/C photoanode was capable of oxidizing benzyl alcohol and its derivatives to their corresponding aldehydes at a selectivity of 100%.

In 2020, Ye, Yan, and Xiang *et al.* conceived a radical relay strategy and successfully coupled water oxidation with the selective oxidation of benzyl alcohol derivatives (**1a**, **1d**, **1j**, **1l**, & **1m**) in a PEC.[55] The photoanode they adopted was a ternary composite consisting of an ultrathin Co-based layered double hydroxide, graphene, and a layer of $BiVO_4$ particles (G@U-LDH@BVO). In the preparation of the photoanode, $BiVO_4$ particles were first deposited on an FTO through electrodeposition; after a hydrothermal process, the as-prepared $BiVO_4$ photoanode was finally modified by graphene and U-LDH. The conducting characteristics of graphene facilitate the transfer of photoexcited electrons from U-LDH to $BiVO_4$. Meanwhile, U-LDH can accept the photogenerated holes and catalyze water oxidation. The relayed $^{\cdot}OH$ adsorbed on the surface of U-LDH was key to the selective oxidation of benzyl alcohol derivatives. This radical relay strategy enables the efficient coupling between water splitting and the selective oxidation of organic molecules under mild conditions.[56] Under a neutral condition (8 mL phosphate-buffered saline (PBS) solution + 2 mL MeCN), G@U-LDG@BVO could realize the photoelectrocatalytic oxidation of substituted benzyl alcohols into the corresponding aldehyde products with excellent selectivity (>96%) and production rate (125–188 μmol h^{-1}). For comparison, the results of the photoanode-mediated benzyl alcohol oxidation are summarized in Table 1.

Another example of simple alcohol oxidation was provided by Cha, Goodwin, and Yehezkeli *et al.* using $BiVO_4$ as the photoanode.[57] The oxidation of *n*-butanol (**8**) was catalyzed by alcohol oxidase (AOx), which reduced O_2 to H_2O_2 at the same time. $BiVO_4$ not only afforded the regeneration of oxidant O_2 but also maintained the stability of AOx by timely scavenging the H_2O_2 in the solution. It is worth mentioning that *n*-butyraldehyde (**9**) produced from alcohol oxidation can then undergo an aldol condensation catalyzed by β-alanine and finally be upgraded to 2-ethylhexenal (**10**) within a PEC (Fig. 2), which vividly demonstrated that PECs can be compatible with an enzymatic and homogenous catalyst.

2.1.2 Oxidation of polyhydric alcohols. Having the regioselectivity problem, the selective oxidation of polyhydric alcohols is more complex than simple alcohol oxidation. To the best of our knowledge, no PEC was applied to the oxidation of polyhydric alcohols until 2019, when Liu, Huang, and Xiong *et al.* achieved the selective oxidation of glycerol (**11**) to dihydroxyacetone with a nanoporous $BiVO_4$ photoanode.[58] The preparation of a $BiVO_4$ photoanode included the electrochemical deposition of BiOI nanoflake arrays on a FTO glass and the reaction between BiOI and vanadyl acetylacetone. This preparation yielded porous and interconnected nanoflake $BiVO_4$ arrays which had a monoclinic scheelite structure and mainly exposed (112) facets. The as-prepared $BiVO_4$ photoanode exhibited an excellent performance in the selective oxidation of glycerol. In an acidic medium (pH = 2.0), the value-added

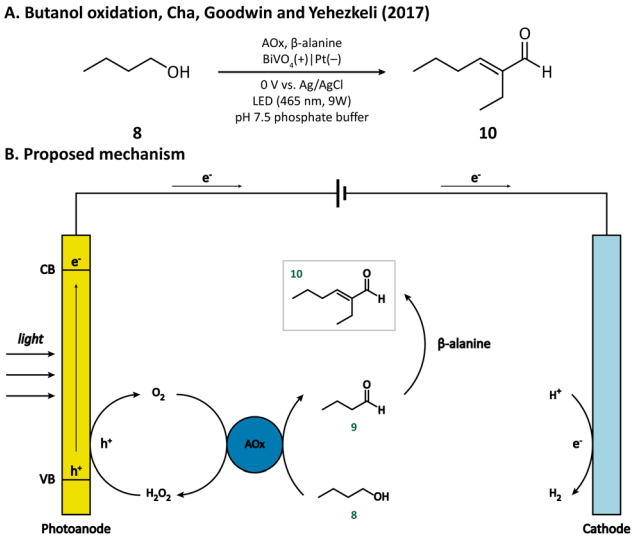

Fig. 2 Photoanode-mediated simple alcohol oxidation coupled with aldol condensation.

product 1,3-dihydroxyacetone (DHA, **12**) can be produced at a rate of 200 mmol m^{-2} h^{-1} under light illumination and external bias (1.2 V *vs.* RHE). Based on the electron spin resonance measurement, the author proposed a direct oxidation mechanism where glycerol is oxidized by photogenerated holes first and then reacts with H_2O to form unstable gem-diol intermediates. But this PEC system suffered from low selectivity (51%), which limits its further application.

Subsequently, many attempts have been made to investigate the performance of a PEC in glycerol conversion.[59–64] For instance, in early 2022, Duan, Li, and co-workers reported the same reaction with a higher selectivity towards DHA (75.4%) by modifying Bi_2O_3 on TiO_2 (Bi_2O_3/TiO_2).[62] The cocatalyst Bi_2O_3, prepared by an electrodeposition-electrooxidation process, could not only improve the light absorption ability of TiO_2 but also facilitate the charge transfer by forming a p–n junction with TiO_2, which greatly enhances the photocurrent density. Unlike the $BiVO_4$ system, the glycerol oxidation on Bi_2O_3/TiO_2 was considered as an *OH radical-mediated process. It was demonstrated by *in situ* Fourier transform infrared spectroscopy and density functional theory (DFT) calculations that glycerol prefers to adsorb over Bi_2O_3 with its middle hydroxyl group and DHA can poorly adsorb on Bi_2O_3, which explained the relatively high selectivity of DHA production. At an external bias of 1.0 V *vs.* RHE, the Bi_2O_3/TiO_2 photoanode sustained glycerol conversion at a rate of 228 mmol m^{-2} h^{-1} when being exposed to light irradiation in an acidic environment (pH = 2.0).

Only two months later, Xiang and Yan *et al.* successfully conducted glycerol oxidation in a neutral medium.[63] They established a ternary photoanode by depositing silver nanoparticles on layered double hydroxide nanosheets grown on TiO_2 arrays (denoted as Ag@LDH@TiO_2). In this ternary photoanode, TiO_2 played the role of harvesting light energy, the LDH nanosheets selectively adsorbed and activated the middle hydroxyl group in glycerol, and the loaded Ag nanoparticles

Table 2 Photoanode-mediated glycerol oxidation

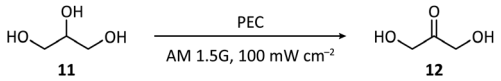

Photoanode	Conditions	Performance	Ref.
$BiVO_4$	1.2 V *vs.* RHE, 0.5 M Na_2SO_4, pH 2.0 H_2SO_4 solution	Photocurrent density: 3.7 mA cm^{-2} DHA selectivity: 51% DHA production: 200 mmol^{-1} m^{-2} FE for DHA production: ≈30%	58
$BiVO_4$	0.7 V *vs.* RHE, 0.1 M $Na_2B_4O_7$ (pH = 2)	DHA selectivity: 15%	59
{010}-$BiVO_4$	1.1 V *vs.* RHE, 0.1 M $Na_2B_4O_7$, pH 2.0 H_2SO_4 solution	Photocurrent density: ≈1.4 mA cm^{-2} DHA selectivity: ≈60%	60
$NiO_x(OH)_y$/W:$BiVO_4$	1.2 V *vs.* RHE, pH 9.3 borate buffer	Photocurrent density: 3.5 mA cm^{-2} DHA selectivity: ≈35% DHA production: 138 mmol^{-1} m^{-2} FE for DHA production: 19%	61
Bi_2O_3/TiO_2	1.0 V *vs.* RHE, 0.5 M Na_2SO_4, pH 2.0 H_2SO_4 solution	Photocurrent density: 0.27 mA cm^{-2} DHA selectivity: 75.4% DHA production: ≈172 mmol^{-1} m^{-2} FE for DHA production: 62.2%	62
Ag@LDH@TiO_2	1.2 V *vs.* RHE, 0.5 M Na_2SO_4	Photocurrent density: 2.12 mA cm^{-2} DHA selectivity: 72.1% DHA production: ≈227 mmol^{-1} m^{-2} FE for DHA production: ≈55%	63
Ta:$BiVO_4$	1.0 V *vs.* RHE, 100 mM H_2SO_4 acetone/H_2O	Photocurrent density: 2.5 mA cm^{-2} DHA selectivity: ≈100% FE for DHA production: 96%	64

facilitated glycerol oxidation by transferring electrons with LDH nanosheets. Using isotopic labelling experiments, the author proposed a mechanism where glycerol first undergoes a dehydration and dehydrogenation process on LDH and then reacts with an *OH radical to form DHA, which was different from the gem-diol mechanism reported in a previous PEC glycerol oxidation system.[58,62] Under neutral conditions (0.5 M Na_2SO_4, pH = 7), glycerol can be converted at a considerable rate (315 mmol m^{-2} h^{-1}) with a DHA selectivity of 72.1%.

More recently, a tantalum-doped $BiVO_4$ (Ta:$BiVO_4$) photoanode was fabricated and applied in glycerol oxidation by Sayama's group.[64] In the fabrication of the Ta:$BiVO_4$ photoanode, $BiVO_4$ was first deposited on a WO_3-coated FTO substrate *via* a spin-coating method and a following calcination; then, a solution containing bismuth oxide, vanadium, and tantalum oxides was spin-coated and calcinated on the as-prepared $BiVO_4$/WO_3/FTO photoanode. Ta atoms were found to be concentrated on the surface of the photoanode by EDS mapping and they were considered to exist in the form of Ta^{5+}. The existence of a Ta-rich overlayer improved the light-harvesting efficiency of $BiVO_4$, which resulted in an enhanced glycerol oxidation photocurrent density compared with that of the bare $BiVO_4$ photoanode. When Ta:$BiVO_4$ was placed under an acidic condition (100 mM H_2SO_4 in acetone/H_2O), the faradaic efficiency of the DHA reached 96% and the selectivity towards DHA was impressively close to 100%, which was significantly higher than those in previous studies (Table 2).

2.2 C–H functionalization

The direct functionalization of a C–H bond can achieve the construction of a carbon–carbon or carbon-heteroatom bond without the independent preparation of reactive functional groups, which is of high atomic and redox efficiency.[65–67] However, the ubiquity and stability of C–H bonds make it challenging to achieve high catalytic activity while maintaining high selectivity.[68] PECOS, harvesting light energy to provide Gibbs energy for C–H activation and using electricity to control the reaction rate, is a promising method to resolve this dilemma. We offer here an overview of the hitherto developed PEC-mediated C–H functionalization methods, including examples of C–H halogenation, oxygenation, amination, phosphorylation, and C–C coupling.

2.2.1 C–H halogenation. The conventional methods for synthesizing organic halides usually require external oxidants[69,70] and harsh reaction conditions,[71,72] which do not meet the goal of sustainable production. As an alternative

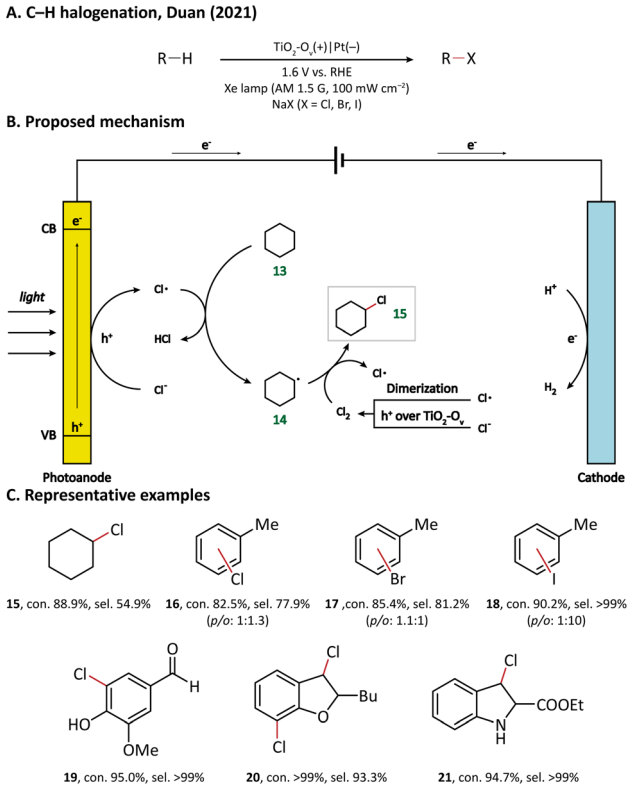

Fig. 3 Photoanode-mediated cyclohexane halogenation.

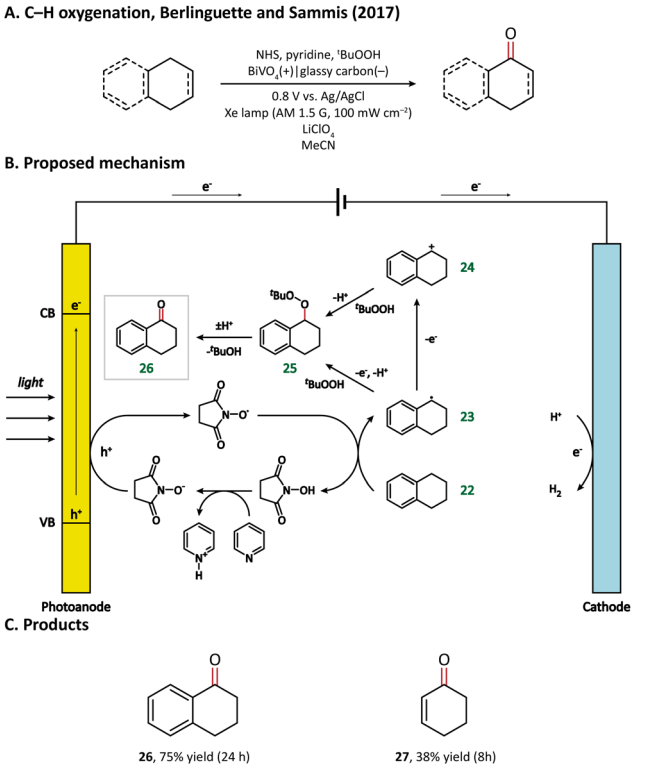

Fig. 4 Photoanode-mediated C–H oxygenation at the α-position of the alkane and arene.

solution, photoelectro-catalytic C–H halogenation was achieved over an oxygen-vacancy-rich TiO_2 (TiO_2–O_v) photoanode by Duan's group in 2021.[73] Oxygen vacancies were introduced to the pristine TiO_2 photoanode *via* an annealing treatment in a H_2 atmosphere. The introduction of oxygen vacancies narrowed the band gap of TiO_2, thereby improving the charge separation efficiency, reducing the electron–hole recombination possibility, and expanding the light absorption range. Moreover, the oxygen vacancies on the surface of TiO_2 played a crucial role in the adsorption of halide anions, which could increase the local halide concentration around the surface of TiO_2 and hence improve its catalytic performance towards C–H halogenation. Taking sea water as the chloride ion source and electrolyte, cyclohexane (**13**) could be converted into chlorocyclohexane (**15**) with a productivity of 412 μmol h^{-1} in a self-powered PEC system. Based on the experimental results, a free-radical mechanism was proposed (Fig. 3). On the surface of TiO_2–O_v, halogen ions adsorbed by the oxygen vacancies are oxidized by photogenerated holes to form halogen radicals, which then activate the cyclohexane (**13**) into a cyclohexyl radical (**14**) and participate in the generation of the final product. The scope of such photoanode-mediated C–H halogenation is not limited to chlorocyclohexane production, TiO_2–O_v can also achieve efficient C–H chlorination, bromination, and iodination of a variety of aromatic and heterocyclic aromatic hydrocarbons (**16–21**).

2.2.2 C–H oxygenation. C–H oxygenation is an attractive strategy for synthesizing value-added oxygenated products (alcohols, aldehydes, and ketones) from cheap alkanes.[74,75] To date, a few PECs adopting this strategy have been successfully established.[76–79]

In 2017, Berlinguette and Sammis *et al.* carried out C–H oxygenation at the α-position of the alkene and arene in a PEC taking $BiVO_4$ as the photoanode.[76] The oxygenation of substrates takes place in an indirect oxidation pathway: photogenerated holes first oxidize an *N*-hydroxysuccinimide anion (NHS^-) into NHS$^\bullet$, which then abstracts the α-H from the substrate (**22**); the as-formed carbon-centered active species (**23**

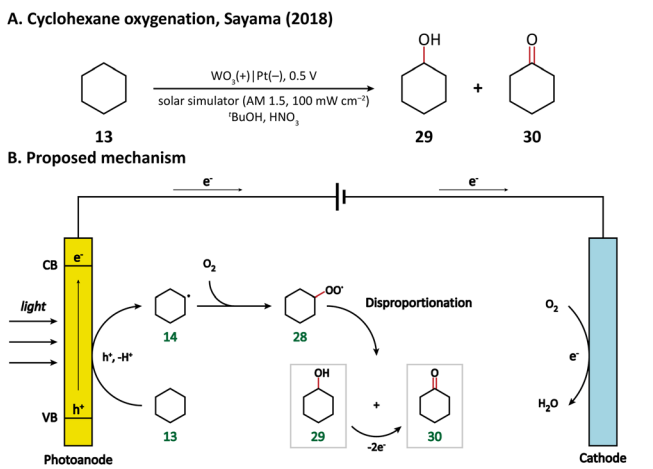

Fig. 5 Photoanode-mediated cyclohexane oxygenation.

& **24**) subsequently react with *tert*-butyl hydroperoxide (^{t}BuOOH) and finally yield oxygenated products (Fig. 4). Notably, the introduction of light energy enabled the reduction of applied bias from 1.8 V in an electrochemical cell to 0.8 V in a PEC, leading to a 60% decrease in energy consumption.

Using porous WO_3 as the photoanode, Sayama's group succeeded in C–H oxygenation of cyclohexane at room temperature and atmospheric pressure.[77] As shown in Fig. 5, the C–H bond in cyclohexane (**13**) is directly activated by the photogenerated holes on the photoanode and the generated cyclohexyl radical (**14**) immediately captures a molecule O_2 in air to form a cyclohexylperoxyl radical (**28**), whose disproportionated reaction yields cyclohexanol (**29**) and cyclohexanone (**30**). Cyclohexanol may also undergo a two-electron oxidation into cyclohexanone. Under simulated-solar light irradiation, cyclohexane could be converted efficiently with a high partial oxidation selectivity of 99%.

Compared with cyclohexane, methane (**31**) has a stronger C–H bond (bond dissociation energy, BDE = 105 kcal mol^{-1}),[80] and hence, is more difficult to activate. The challenging methane oxygenation towards ethylene glycol (EG, **35**) has been accomplished by Xiong and co-workers in a PEC equipped with a monoclinic WO_3 photoanode.[79] Through the hydrothermal method, they successfully grew WO_3 nanobar, nanoplate, and nanoflake arrays on FTO substrates. The facet-dependent performance of WO_3 was studied. It was found that WO_3 nanobars, exhibiting the highest {010} facet ratio, has the best EG productivity and selectivity upon light irradiation in an acidic medium (pH 2.0 H_2SO_4 solution), which may be due to the high reactivity of $^{\bullet}$OH bound on {010} facets. A plausible mechanism proposed by the author is illustrated in Fig. 6. First, the H_2O molecule is oxidized by the photoanode to generate the surface-bound $^{\bullet}$OH. Methane (**31**) is then activated by $^{\bullet}$OH and $^{\bullet}CH_3$ (**32**) is formed. The combination of $^{\bullet}$OH and $^{\bullet}CH_3$ leads to the generation of CH_3OH (**33**), which subsequently undergoes a similar activation process to form $^{\bullet}CH_2OH$ (**34**). The coupling between two $^{\bullet}CH_2OH$ yields the final product EG (**35**). The byproduct ethane (**36**) may result from the coupling of two $^{\bullet}CH_3$ radicals.

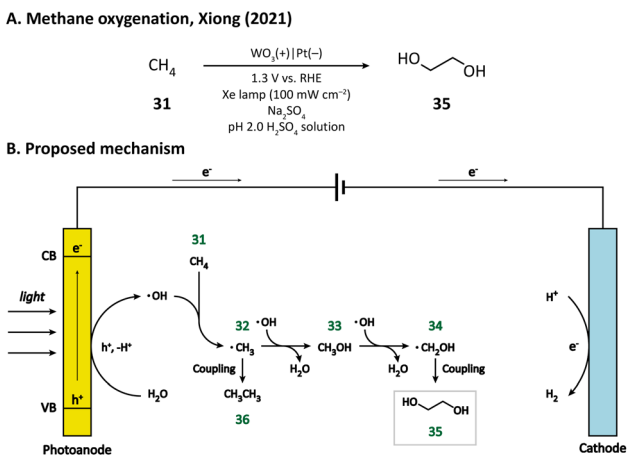

Fig. 6 Photoanode-mediated methane oxygenation.

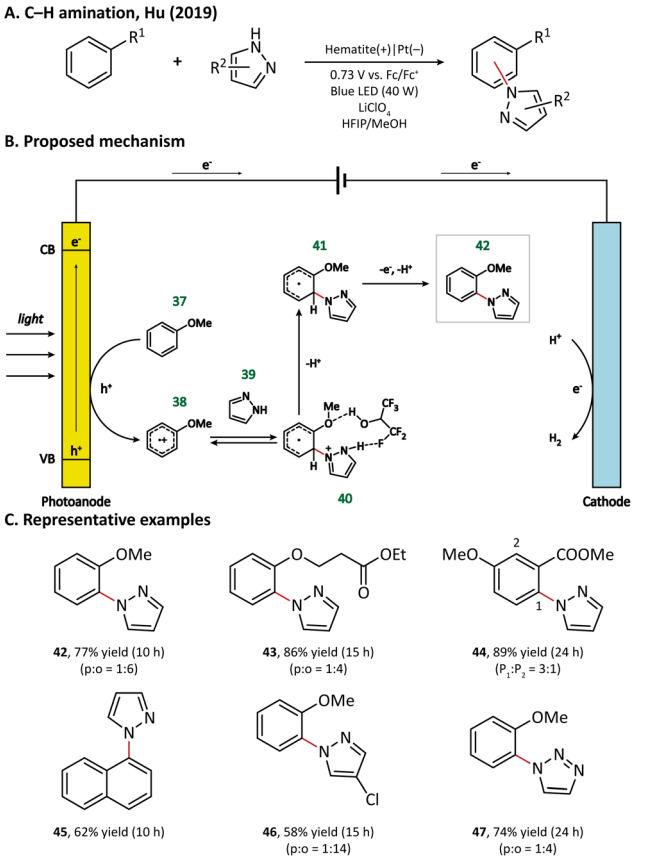

Fig. 7 Photoanode-mediated arene amination.

2.2.3 C–H amination. Ubiquitous in natural and man-made products, nitrogen-containing organic compounds have a broad scope of applications.[81–83] Synthesizing these compounds from C–H amination is very strategically attractive.[84,85] However, the conventional methods adopting this strategy are suffering from harsh reaction conditions (excess oxidant, elevated temperature, or high applied potential)[86–89] or poor catalyst stability.[90,91] A more sustainable solution was devised by Hu and co-workers in 2019.[92] Inspired by the similar theoretical oxidizing power of the hematite valence band and acridinium, the author adopted nanoporous hematite as the photoanode and achieved the C–H amination of various arenes with serval kinds of nitrogen nucleophiles (**42–47**). Taking $LiClO_4$ as the electrolyte, the hematite photoanode was capable of sustaining the long-time (10 h) C–H amination of anisole with an acceptable yield (77%) in hexafluoroisopropanol (HFIP) and MeOH co-solvent at a low external bias of 0.73 V *vs.* Fc/Fc^+ without the need of an adscititious oxidant.

Surprisingly, an unusual ortho selectivity could be obtained in this hematite-mediated PEC, which was speculated to be originated from the interactions between the radical cations and the solvent HFIP. Considering these experimental results, the author proposed a mechanism for C–H amination (Fig. 7). To begin with, the electron-rich arene (**37**) is directly oxidized by the photogenerated holes to form a radical cation (**38**). With the help of the HFIP molecule, the nucleophilic azole (**39**) attacks

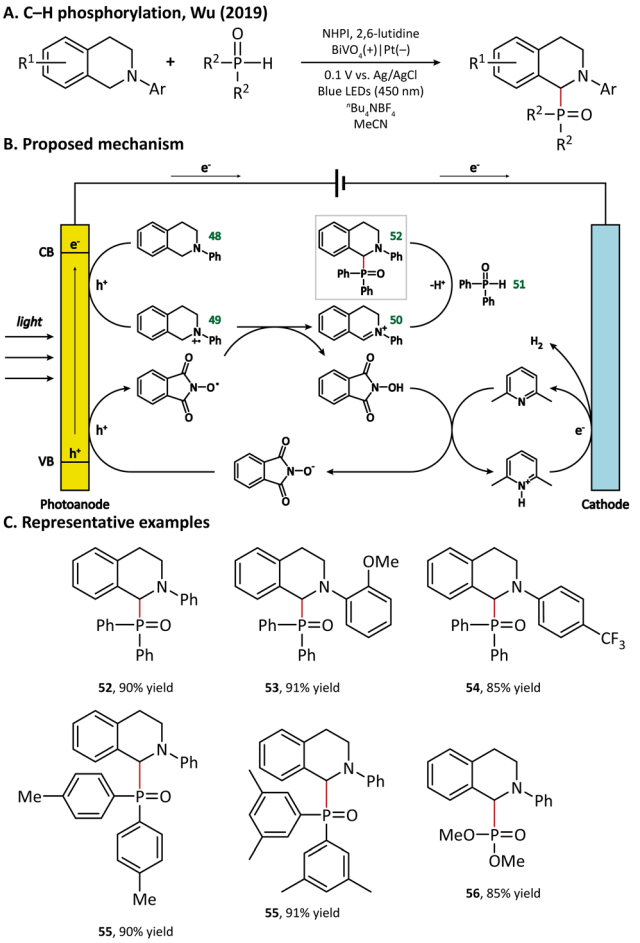

Fig. 8 Photoanode-mediated C–H phosphorylation.

the ortho position of arene and generates an adduct **40**, which then loses one electron and two protons to form the final product **42**.

2.2.4 C–H phosphorylation. Organophosphorus compounds are important structural motifs that widely exist in agrochemistry, material chemistry, and biochemistry.[93,94] In 2019, Wu and co-workers achieved the P–H/C–H cross-coupling in PEC and EC systems with hydrogen evolution.[95] In contrast to traditional synthetic methods (*e.g.*, transition metal catalysis,[96,97] chemical oxidation,[98,99] and photocatalysis[100,101]), this work showed that the fabricated $BiVO_4$ PEC was able to produce a series of C–P bond derivatives (**52–56**) in good to excellent yields without the aid of any external oxidants or metal catalysts. The applied bias to produce a (photo) current of 5.0 mA was 0.1 V and 1.5 V in the $BiVO_4$ photoelectrochemical system and the glassy carbon electrochemical system, respectively. These potentials afforded the target products with very similar yields after 12 h of (photo) electrolysis, indicating that PECOS is a more energy-saving method than the traditional electrochemical organic synthesis.

A plausible mechanism for photoelectrochemical P–H/C–H cross-coupling is outlined in Fig. 8. The holes reach the surface of $BiVO_4$ to oxidize **48** into a radical cation intermediate (**49**). Then, the *N*-hydroxyphthalimide (NHPI) deprotonated by 2,6-lutidine goes through an anodic oxidation to give the corresponding PINO radicals. Next, the PINO radical extracts a hydrogen atom from **49** to regenerate NHPI, and **49** is further oxidized to afford an iminium ion intermediate (**50**), which reacts with diphenyl-phosphine oxide (**51**) *via* a nucleophilic attack to enable the formation of the final product with a C–P bond (**52**).

2.2.5 C–C coupling. C–C coupling is an effective approach for the construction of organic compounds with complex skeletons.[102,103] In conventional organic synthesis, the formation of a C–C bond is usually accompanied by discarding a huge leaving group, which is of a low atomic economy.[68] In contrast, the coupling between two carbon radicals generated from C–H activation only wastes two hydrogen atoms, thus making it a greener synthetic strategy. In 2022, Wu and Kim *et al.* reported the synthesis of *N*-bearing fused rings adopting this strategy in a PEC with a $BiVO_4$ photoanode.[104] Under blue LED irradiation, the substrates 2-phenyl-1,2,3,4-tetrahydroisoquinoline (**48**) and malononitrile (**63**) could be coupled into 5,12a-dihydroindolo

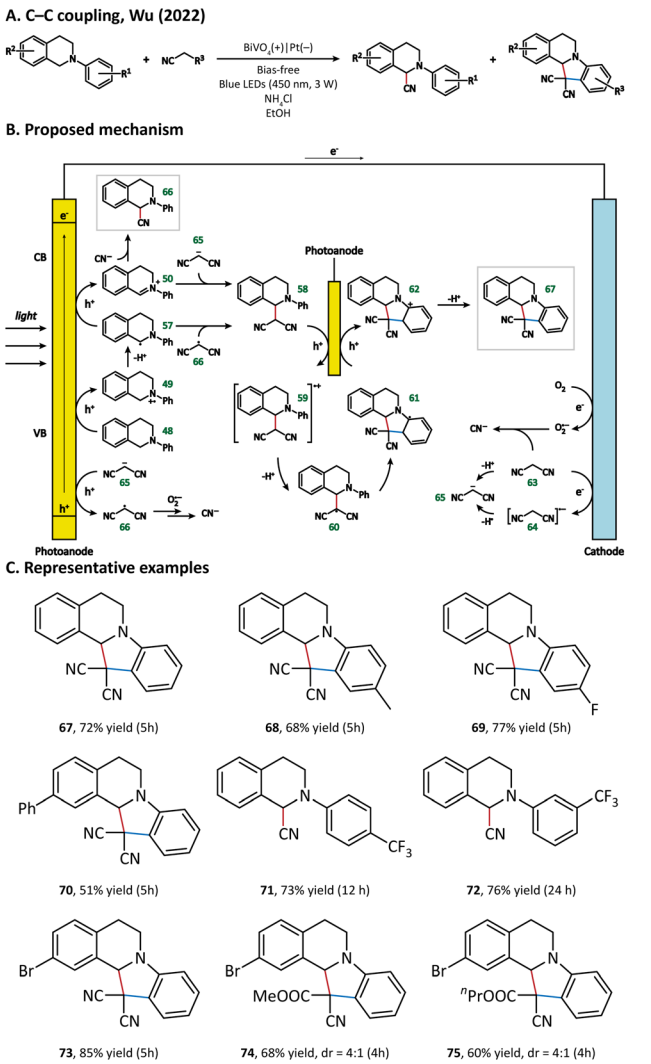

Fig. 9 Photoanode-mediated C–C coupling.

[2,1-*a*]isoquinoline-12,12(6*H*)-dicarbonitrile (**67**) with a yield of 72% even without external bias. Meanwhile, 2-phenyl-1,2,3,4-tetrahydroisoquinoline-1-carbonitrile (**66**) was found to be the byproduct. $BiVO_4$ exhibited a similar reactivity after ten cycles of catalysis, indicating long-term stability. The substrate scope was further expanded by investigating the coupling between the derivatives of **48** or **63**. **68–75** are the representative examples of products obtained by this method.

The possible reaction pathways are illustrated in Fig. 9. Generally speaking, **48** loses its electron(s) at the photoanode and forms either a radical (**57**) or cation (**58**) intermediate. In the meantime, **63** undergoes a deprotonation process at the cathode to generate a malononitrile anion **65**. **65** could be oxidized by the photoanode to give the malononitrile radical **66**. The intermediate product **58** is generated either from a radical process (**57** + **66**) or from an ion process (**50** + **65**). After complex oxidation, deprotonation, and radical cyclization processes, **58** is finally converted into *N*-containing fused ring compound **67**. The generation of byproduct **66** originated from the coupling of **50** and cyanide, which is produced *via* the oxidation of **63** or **66** by a superoxide anion reduced from the O_2 molecule at the cathode.

2.3 Oxidation of other organic compounds

2.3.1 Furan. The first work using a PEC for furan oxidation was presented by Sayama's group in 2017, where a $BiVO_4/WO_3$ composite was utilized as a photoanode.[105] WO_3 and $BiVO_4$ were sequentially deposited onto the FTO substrate through the spin-coating method. Scanning electron microscopy revealed that the $BiVO_4/WO_3$ photoanode displayed a rough and porous morphology. The oxidation was carried out in a mixture of MeCN and MeOH, taking Et_4NBF_4 and Et_4NBr as the electrolyte. When the system was irradiated by using a solar simulator (AM 1.5 G, 100 mW cm^{-2}), furan (**76**) could be converted into 2,5-dimethoxy-2,5-dihydrofuran (DMDF, 77) with a faradaic efficiency (>99%) at a low bias (0.1 V *vs.* SHE). It was found that the addition of Et_4NBr is crucial for the effective production of DMDF and Et_4NBr cannot be replaced by Br_2, indicating that furan was probably not oxidized by Br_2 but by a Br^+-like species. Based on these results, the author proposed a Br^+/Br^--mediated indirect oxidation mechanism for furan conversion (Fig. 10).

In 2021, Kuang's group improved this reaction by using a perovskite single-crystal thin film (SCTF) as the photoanode.[106] A space-limited crystallization method was applied to obtain the *in situ* growth of a methylammonium lead bromide ($MAPbBr_3$) SCTF on an FTO/TiO_2 substrate.[107,108] Later, the surface defects of the $MAPbBr_3$ SCTF were greatly passivated by the deposition of an ultrathin Al_2O_3 layer, which effectively enhanced the stability of the photoanode. After depositing a Ti^{3+}-rich titanium layer, the stability and PEC performance of the photoanode were further advanced. The maximum photocurrent density of the as-prepared $MAPbBr_3$ SCTF/Al_2O_3/Ti photoanode was up to 7.8 mA cm^{-2} at 0.8 V *vs.* Ag/AgCl, which was significantly higher than that reported by Sayama's group (0.55 mA cm^{-2} at 0.5 V *vs.* SHE). Besides, this photoanode was capable of maintaining its reactivity after 6 h of continual DMDF production at an applied potential of 0.2 V *vs.* AgCl, indicating that it possessed eminent stability towards PECOS. DFT simulations unveiled the advantageous Br adsorption and significant charge transfer on the Ti^{3+}-titanium layer, which explained the excellent PEC performance of the $MAPbBr_3$ SCTF/Al_2O_3/Ti photoanode.

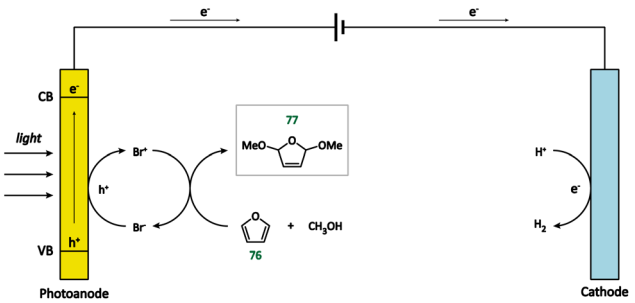

Fig. 10 Photoanode-mediated furan oxidation.

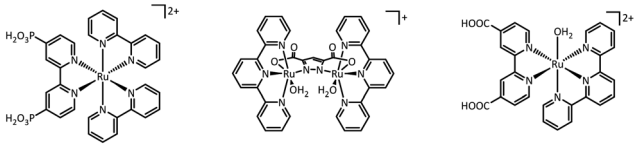

Fig. 11 Dyes and catalysts used in photoanode-mediated sulfide oxidation.

2.3.2 Sulfides. Early in 2015, Llobet and Palomares *et al.* realized the oxidation of sulfide into sulfoxide in a PEC at a proof-of-concept level.[109] Oxidation was performed on a dye(**78**)-sensitized TiO_2 photoanode together with a homogenous ruthenium-based catalyst (**79**) (the molecular structures of the dyes and catalysts used in photoanode-mediated sulfide oxidation are illustrated in Fig. 11). Even though a high faradaic efficiency for H_2 evolution (89%) could be obtained, the yield of sulfoxide is very low (*ca.* 0.6%).

One year later, Sun's group developed a molecular ruthenium catalyst (**80**) modified hematite photoanode and applied it to the PEC oxidation of thioanisole in aqueous solutions (pH = 3 potassium hydrogen phthalate buffer).[44] At an applied bias of 1 V *vs.* RHE, the photocurrent density for thioanisole oxidation reached around 300 μA cm^{-2}. Long-term photoelectrolysis exhibited a high faradaic efficiency of 93% and benzyl methyl sulfoxide was found to be the only organic product.

The performance of the hematite photoanode was further improved by Zhao, Chen, and Zhang *et al.* in 2021, where MeCN rather than water was used as the solvent.[110] In the preparation of the photoanode, FeOOH was first hydrothermally grown on a clean FTO substrate; then, a temperature-programmed annealing treatment transformed FeOOH into hematite with a nanowire morphology. It was found that a bare hematite photoanode is able to produce methyl phenyl sulfoxide (**81**) from thioanisole in an efficient manner. The author also investigated the sulfoxidation reaction of para-substituted

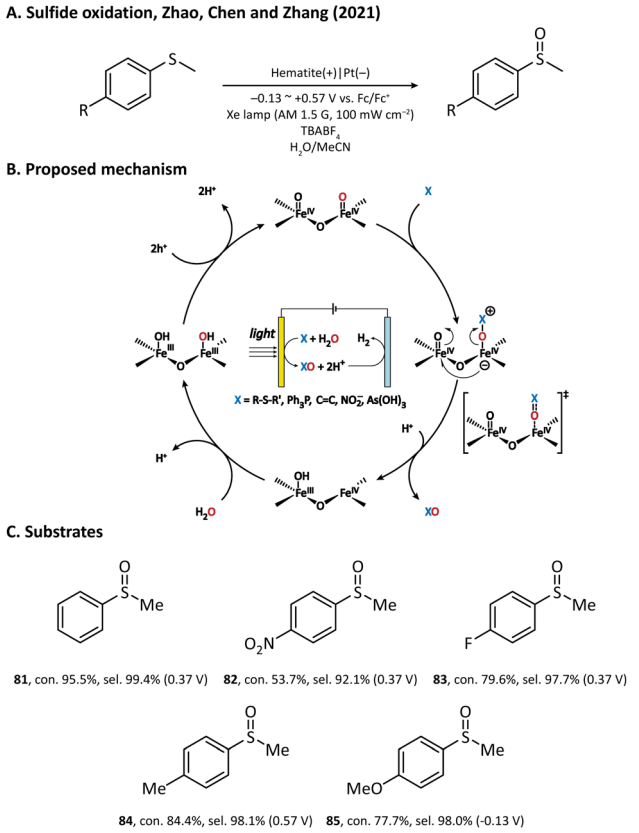

Fig. 12 Hematite-mediated oxygen atom transfer reaction.

thioanisole derivatives (**82–85**) and discovered a negative correlation in the Hammett plot, which suggested that the rate-limiting step of hematite-mediated sulfoxidation has a positively charged transition state.[111,112] Based on the experimental results and theoretical calculations, an oxygen atom transfer (OAT) mechanism was established (Fig. 12). Upon light illumination, holes are generated and trapped on the surface of hematite to form two adjacent Fe^{IV}=O sites. After that, the nucleophilic substrate attacks the oxygen atom of one Fe^{IV}=O site. The following step is the rate-determining step, where an oxygen atom is transferred from the hematite surface to the substrate with a concerted two-hole transfer after a positively charged transition state. Finally, the oxygen vacancy left on the surface is replenished by the water molecules in the solvent and the catalytic cycle is completed. Notably, with such an OAT mechanism, the hematite photoanode can also be applied to other organic transformations such as PPh_3 oxygenation and C=C epoxidation, but we will not introduce them in detail in this review.

3. (Photo)cathode-mediated organic synthesis

Compared with the widely researched photoanode-mediated organic synthesis, the potential of a PEC cathode in organic synthesis is nearly undeveloped. But there are, indeed, a few published studies trying to cultivate (photo)cathode-mediated

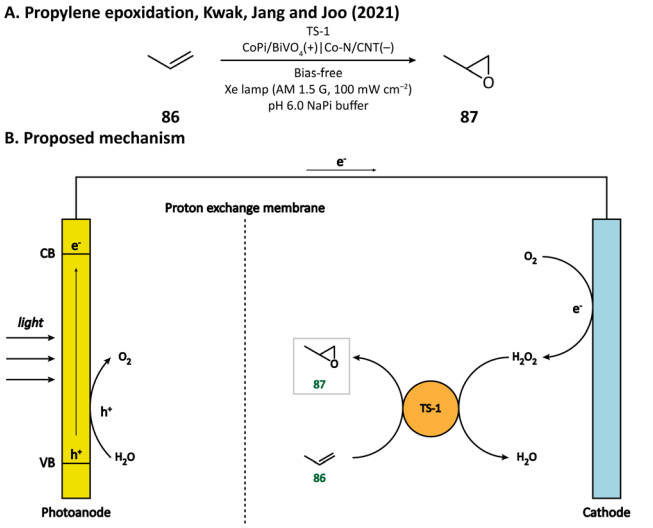

Fig. 13 Cathode-mediated *in situ* H_2O_2 generation for propylene epoxidation.

organic synthesis. Some of them utilize the electron transported from the photoanode for *in situ* H_2O_2 generation[113–115] or cofactor regeneration[48,115,116] to accomplish the oxidation or reduction of organic substrates, while others adopt a photocathode as an electron source.[117,118]

3.1 Cathode-mediated *in situ* H_2O_2 generation

H_2O_2 is a powerful, environmentally benign oxidizing agent because it has considerable oxidation potential (H_2O_2/H_2O: +1.76 V *vs.* NHE)[119,120] and does not generate toxic reduction products. It has been reported that heterogenous catalyst titanium silicalite-1 (TS-1) has the capacity of using H_2O_2 to selectively epoxidize propylene (**86**).[121,122] The current method for H_2O_2 production, however, is the inefficient anthraquinone process which meanwhile produces organic waste.[123] In 2021,

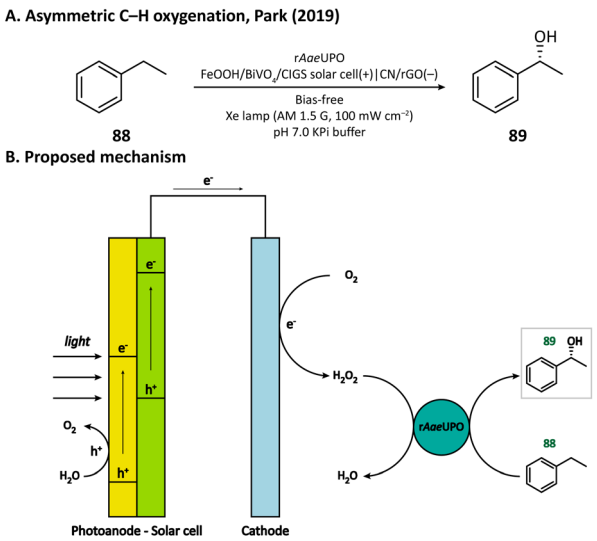

Fig. 14 Cathode-mediated *in situ* H_2O_2 generation for asymmetric C–H oxygenation.

Kwak, Jang, and Joo *et al.* presented a bias-free PEC system where *in situ* photoelectrocatalytic H_2O_2 generation was coupled with propylene epoxidation mediated by TS-1.[114] In this system, the photoanode consisted of a $BiVO_4$ film for light harvesting and cobalt phosphate (CoPi) deposition as an oxygen evolution catalyst; the cathode was made of carbon nanotubes with atomically dispersed Co–N_x sites (Co–N/CNT), which enabled the selective reduction of O_2 to H_2O_2 (Fig. 13). When TS-1 was dispersed in the cathodic electrolyte (pH 6.0 NaPi buffer), the PEC managed to continuously produce propylene oxide (**87**) at a rate of 11.8 μmol h^{-1} with a selectivity higher than 99%. This work demonstrated that it is practical to carry out propylene epoxidation in a green and sustainable manner by coupling PEC-mediated *in situ* H_2O_2 generation with heterogeneous catalysis.

Besides heterogeneous catalysts, heme-dependent enzymes, especially unspecific peroxygenases (UPOs), also have the ability to transfer the oxygen atom in H_2O_2 to organic substrates.[124] Therefore, UPOs should be able to cooperate well with a PEC in the oxidation of organic compounds. In fact, a recombinant peroxygenase from *Agrocybe aegerita* (rAaeUPO) has been used in a PEC for the C–H oxygenation of ethylbenzene (**85**) by Park's group in 2019.[113] In their PEC system, the cathode was a graphitic carbon nitride (CN)/reduced graphene oxide (rGO) hybrid film. The cathode-mediated *in situ* H_2O_2 generation was powered by a FeOOH/$BiVO_4$–Cu(In, Ga)Se_2 photoanode-photovoltaic tandem structure which provided sufficient photovoltage. By carefully tuning the loading amount of rGO, the production rate of H_2O_2 was optimized, which maximized the conversion rate of ethylbenzene and maintains the activity of rAaeUPO. Upon illumination, (*R*)-1-phenylethanol (**89**) was produced at a rate of 0.89 mM h^{-1} with an enantiomeric excess (ee) value higher than 99% in a pH 7.0 KPi buffer, indicating the successful cooperation between the PEC and the enzyme (Fig. 14).

Recently, Park's group provided another example by using anthraquinone-2-carboxylic acid (AQC) anchored carbon fiber paper (CFP) as the cathode.[115] They adopted Zr-doped hematite as the photoanode, which had the capability of converting poly(ethylene terephthalate) (PET) microplastics into chemical fuels in an alkaline medium (5 M NaOH). The electron extracted from PET is transferred to the cathode and reduces the anchored AQC into $AQCH_2$, which then reacts with O_2 and realizes the *in situ* H_2O_2 generation in a pH 6.0 KPi buffer (Fig. 16). With the help of rAaeUPO, the oxygen atom in H_2O_2 could be transferred into a variety of organic substrates such as ethylbenzene, cyclohexane, tetralin, and *cis*-β-methylstyrene (**92**).

3.2 Cathode-mediated cofactor regeneration

Having extraordinary catalytic activity and selectivity, redox enzymes are ideal catalysts for redox reactions in organic synthesis.[125,126] Nevertheless, many redox enzymes can only reduce organic substrates in the presence of expensive cofactors, which limits their applications in industrial production.[127,128] Regenerating cofactors from their oxidized forms during the reaction can not only sustain the reduction of organic substrates but also minimize the amount of cofactor addition.

In 2018, Park's group employed this strategy for the production of L-glutamate (**91**) in a PEC system.[116] A tandem structure of light-absorbing layers (FeOOH/$BiVO_4$ photoanode and perovskite solar cell) was constructed to generate the bias for the cathode reaction. On the surface of the carbon nanotube (CNT) film cathode, the electron is transferred to an Rh-based electron mediator **M** ($[Cp^*Rh(bpy)H_2O]^{2+}$, Cp^* = C_5Me_5, bpy = 2,2′-bipyridine), which then realizes the regeneration of

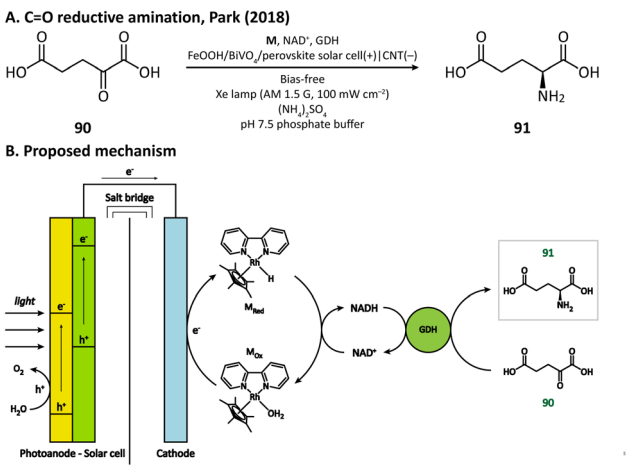

Fig. 15 Cathode mediated cofactor regeneration for C=O reductive amination.

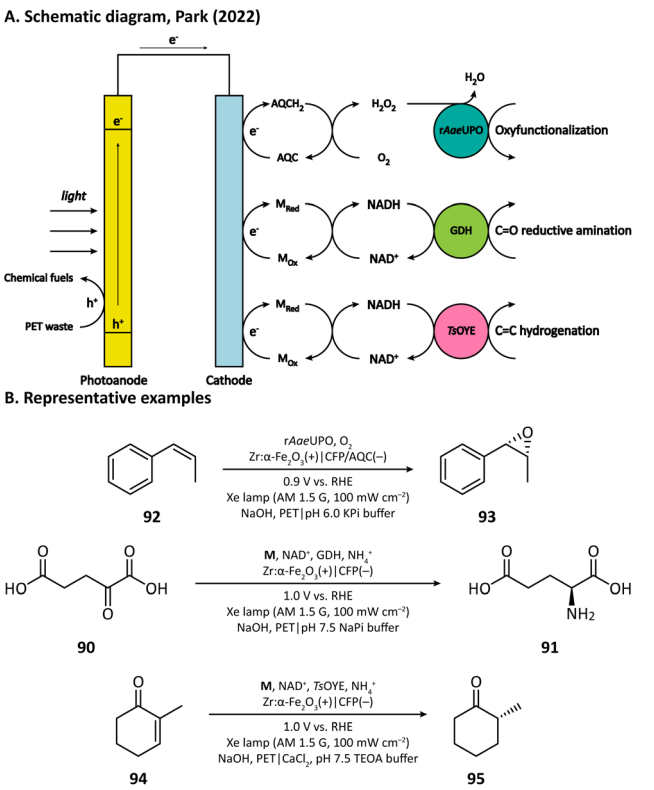

Fig. 16 PET conversion coupled with cathode-mediated biosynthesis.

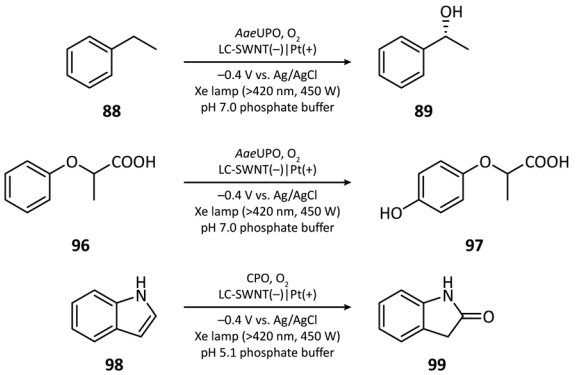

Fig. 17 Photocathode-mediated C–H oxygenation.

nicotinamide adenine dinucleotide (NADH) by reducing NAD^+. The rapid rate of NADH regeneration enabled glutamate dehydrogenase (GDH) to efficiently convert α-ketoglutarate (**90**) into L-glutamate at an initial rate of 2.4 mM h^{-1} in a pH 7.5 phosphate buffer, which was comparable to the production rate obtained in the enzymatic NADH recycling system (Fig. 15).

Cathode-mediated cofactor regeneration has also been coupled with the aforementioned PET conversion by Park's group.[115] **M** was also used as the mediator for the electron transfer between the bare CFP cathode and NAD^+. The regenerated NADH can participate in either the reductive amination of C=O bonds catalyzed by GDH or the hydrogenation of C=C bonds driven by the old yellow enzyme (OYE) (Fig. 16).

3.3 Photocathode-mediated organic synthesis

The first photocathode-mediated PECOS was reported by Park's group in 2017.[117] In this work, the photocathode was prepared by anchoring flavin molecules on the surface of a single-walled carbon nanotube (SWNT) cathode. Under illumination, photosensitive flavin molecules are excited and then converted to their reduced form by receiving electrons from an SWNT cathode. Reduced flavins facilitate the charge transfer between SWNTs and O_2 thereby decreasing the overpotential of O_2 reduction. When luminchrome (LC), a kind of flavin derivative, was immobilized on the surface of SWNTs, O_2 was reduced to H_2O_2 at −0.32 V *vs.* Ag/AgCl with a photocurrent density of −1.42 mA cm^{-2}, which was better than the performance of pristine SWNTs (−0.49 V *vs.* Ag/AgCl and −0.87 mA cm^{-2}). By coupling photocathode-mediated H_2O_2 generation with proper peroxygenase-catalyzed reactions, the oxidation of alkane (**88**), arene (**96**), and indole (**98**) in phosphate buffer was respectively achieved (Fig. 17).

In 2021, Wu's group developed an $Sb_2(S, Se)_3$ photocathode for the selective functionalization of aryl halide.[118] The $Sb_2(S, Se)_3$ photocathode had an ultra-narrow band gap (1.20 eV) and a rod-like structure with high surface area, which were beneficial for the light absorption performance in the visible and near-infrared region and for the electron and mass transportation ability, respectively. An organic photocatalyst *N*,*N*-bis(2,6-ddiisopropylphenyl)perylene-3,4,9,10-bis(dicarboximide) (PDI) was introduced in the electrolyte to promote the electron transfer

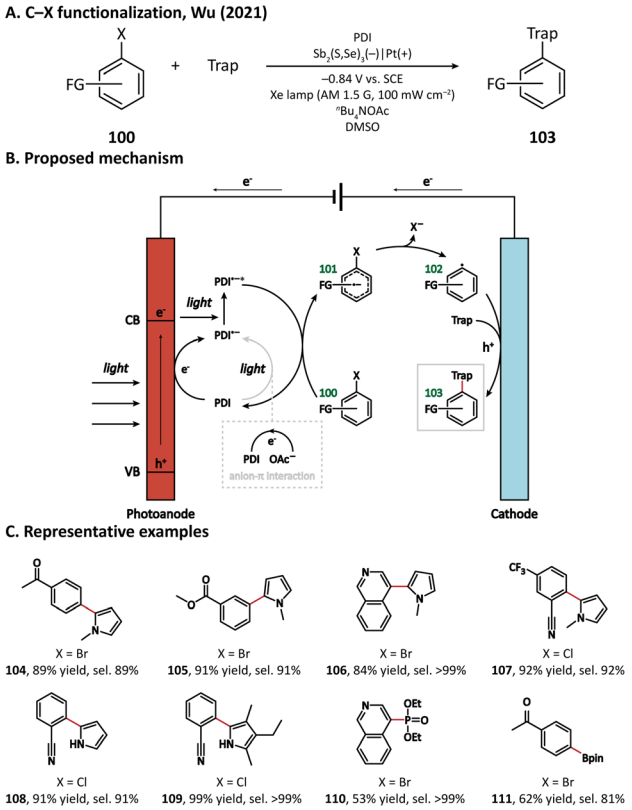

Fig. 18 Photocathode-mediated C–X activation.

between the photocathode and aryl halides. It was found that light and PDI played crucial roles in the catalytic activity, and $^nBu_4NAcO$-containing DMSO was the best reaction medium. Under optimized reaction conditions, 4-bromoacetophenone could be activated and coupled with *N*-methyl pyrrole with an excellent yield of 89% (Fig. 18, **104**), which was much higher than that in photocatalytic and electrophotocatalytic C–X activation mediated by PDI, demonstrating the superiority of this coupled PEC-photocatalysis (c-PEC/PC) system. The substrate scope was also explored. It turned out that such c-PEC/PC was tolerant to a broad scope of aryl halides and trapping agents (**105–111**).

A plausible mechanism for this photocathode-mediated C–X functionalization is displayed in Fig. 18. Upon light illumination, electrons in $Sb_2(S, Se)_3$ are excited from the valence band to the conduction band. The anion-π interaction between the electrolyte anion OAc^- and photocatalyst PDI makes PDI easier to be oxidized. PDI can either be reduced by the photogenerated electron at the surface of the photocathode or accept an electron from OAc^- to form $PDI^{\cdot-}$, which can be further excited by a photon into the more reductive $PDI^{\cdot-}$*. $PDI^{\cdot-}$* then transfers one electron to the aryl halide (**100**), leading to the formation of a radical anion intermediate (**101**). After that, the C–X bond breaks heterolytically, forming an aryl radical (**102**). The aryl radical subsequently reacts with the trapping reagent and loses one electron at the anode to yield the coupling product (**103**).

4. Conclusions and perspectives

In this review, we summarize recent advances in photoelectrochemical alcohol oxidation, C–H functionalization, and (photo) cathode-mediated organic synthesis. Compared with electrochemical systems, PEC systems are still in their infancy but offer prospects for the evolution of solar-induced organic transformations towards better, cheaper, higher efficiency, and sustainable alternative reaction methodologies. Following on from here are four major aspects that will enable photoelectrochemical organic transformations to become a broad subject of interest in the future:

(1) In conventional photoelectrochemical setups, typically, electrode distances range from millimeters to centimeters. The PEC reaction efficiency could be affected by the inefficient mixing of the persistent radical and transient radical. Therefore, how to enhance substrate diffusion will be the key problem of PECOS. (I) The extremely thin interelectrode gap would prevent active intermediate decomposition, selectively producing the target product. Considering this aspect, new PEC devices should be developed to minimize electrode spacing and improve reaction efficiency. (II) In heterogeneous catalysis, the porous nanocatalyst formed on a photoanode can increase the exposure of active sites. The active intermediates produced on the catalyst surface can accelerate the diffusion of thesubstrate during photoelectrolysis.

(2) Heterogeneous catalysis has attracted more attention from researchers due to the tunability of the catalyst structure, morphology and size. From the perspective of economic resources, heterogeneous catalysis avoids the separation process, reduces the cost of catalysts, and realizes recyclable applications. In the future, various catalysts can be modified on the surface of the photoelectrode to generate high-value-added chemicals. For example, high surface area nanopores can be deposited on the photoanode by atomic layer deposition, chemical synthesis, and chemical vapor deposition, which can play a vital role in various organic transformations with enhanced efficiency.

(3) Transition metal catalysis plays an important role in biochemistry and medicinal chemistry, but its large-scale production is limited by harsh reaction conditions. At present, great progress has been made in electrochemical transition metal catalysis, but not in photoelectrochemical transition metal catalysis. Transition metal catalyst deposition on photoanodes can potentially add more value to this process as cocatalysts can offer additional oxidation or reduction active sites. In the future, photoelectrochemical metal catalysis is a new technology for organic synthesis.

(4) Asymmetric catalysis has always been the most challenging research area and the focus of organic chemists. At present, many factors are hindering the development of electrochemical asymmetric catalysis. For example, chiral catalysts are easy to inactivate during electrolysis. The bottleneck of this field is to develop appropriate catalysts that can withstand electrochemical oxidation and provide stereoselective control. In contrast, photoelectrochemical asymmetric catalysis has unique advantages due to its lower bias voltage, which can effectively prevent peroxidation, ligand deactivation, and other problems. In the future, the development of photoelectrochemical asymmetric catalysis will add new vitality to organic synthesis methodology.

Conflicts of interest

There are no conflicts to declare.

Acknowledgements

The authors acknowledge financial support from the National Key R&G Program of China (2021YFA1200302, Z. Y. T.), Strategic Priority Research Program of the Chinese Academy of Sciences (XDB36000000, Z. Y. T.), and National Natural Science Foundation of China (92056204, 21890381 and 21721002, Z. Y. T.).

Notes and references

1 S. Dong, J. Feng, M. Fan, Y. Pi, L. Hu, X. Han, M. Liu, J. Sun and J. Sun, *RSC Adv.*, 2015, **5**, 14610–14630.
2 H. Mai, D. Chen, Y. Tachibana, H. Suzuki, R. Abe and R. A. Caruso, *Chem. Soc. Rev.*, 2021, **50**, 13692–13729.
3 Z. Bi, R. Guo, X. Hu, J. Wang, X. Chen and W. Pan, *Nanoscale*, 2022, **14**, 3367–3386.
4 X. Yang and D. Wang, *ACS Appl. Energy Mater.*, 2018, **1**, 6657–6693.
5 J. Li, X. Han, D. Wang, L. Zhu, M. Ha-Thi, T. Pino, J. Arbiol, L. Wu and M. N. Ghazzal, *Angew. Chem., Int. Ed.*, 2022, **61**, e202210242.
6 J. Li, X. Gao, L. Zhu, M. N. Ghazzal, J. Zhang, C. Tung and L. Wu, *Energy Environ. Sci.*, 2020, **13**, 1326–1346.
7 T. Hisatomi, J. Kubota and K. Domen, *Chem. Soc. Rev.*, 2014, **43**, 7520–7535.
8 J. Li and N. Wu, *Catal. Sci. Technol.*, 2015, **5**, 1360–1384.
9 P. Chen, Y. Zhang, Y. Zhou and F. Dong, *Nano Mater. Sci.*, 2021, **3**, 344–367.
10 G. Hilt, *ChemElectroChem*, 2020, **7**, 395–405.
11 A. Landman, H. Dotan, G. E. Shter, M. Wullenkord, A. Houaijia, A. Maljusch, G. S. Grader and A. Rothschild, *Nat. Mater.*, 2017, **16**, 646–651.
12 C. Ros, T. Andreu and J. R. Morante, *J. Mater. Chem. A*, 2020, **8**, 10625–10669.
13 J. P. Barham and B. König, *Angew. Chem., Int. Ed.*, 2020, **59**, 11732–11747.
14 Y. Chen, W. Deng, J. Guo, R. Ci, C. Zhou, B. Chen, X. Li, X. Guo, R. Liao, C. Tung and L. Wu, *J. Am. Chem. Soc.*, 2022, **144**, 20975.
15 H. Huang, K. A. Steiniger and T. H. Lambert, *J. Am. Chem. Soc.*, 2022, **144**, 12567–12583.
16 A. Fujishima and K. Honda, *Nature*, 1972, **238**, 37–38.
17 I. Roger, M. A. Shipman and M. D. Symes, *Nat. Rev. Chem.*, 2017, **1**, 0003.
18 C. Jiang, S. J. A. Moniz, A. Wang, T. Zhang and J. Tang, *Chem. Soc. Rev.*, 2017, **46**, 4645–4660.

19 S. Wang, G. Liu and L. Wang, *Chem. Rev.*, 2019, **119**, 5192–5247.
20 X. Chang, T. Wang and J. Gong, *Energy Environ. Sci.*, 2016, **9**, 2177–2196.
21 M. A. Lumley, A. Radmilovic, Y. J. Jang, A. E. Lindberg and K. S. Choi, *J. Am. Chem. Soc.*, 2019, **141**, 18358–18369.
22 V. Kumaravel, J. Bartlett and S. C. Pillai, *ACS Energy Lett.*, 2020, **5**, 486–519.
23 Y. Liu, S. Bai, F. Wang and Y. Chen, *Environ. Chem. Lett.*, 2022, **20**, 1169–1192.
24 S. Xu and E. A. Carter, *Chem. Rev.*, 2019, **119**, 6631–6669.
25 C. Li, T. Wang, B. Liu, M. Chen, A. Li, G. Zhang, M. Du, H. Wang, S. F. Liu and J. Gong, *Energy Environ. Sci.*, 2019, **12**, 923–928.
26 R. Kamata, H. Kumagai, Y. Yamazaki, M. Higashi, R. Abe and O. Ishitani, *J. Mater. Chem. A*, 2021, **9**, 1517–1529.
27 S. Navarro, M. Virginie, J. Bonin, M. Robert, R. Wojcieszak and A. Y. Khodakov, *Nat. Rev. Chem.*, 2021, **5**, 564–579.
28 W. J. Dong, I. A. Navid, Y. Xiao, T. H. Lee, J. W. Lim, D. Lee, H. W. Jang, J. L. Lee and Z. Mi, *J. Mater. Chem. A*, 2022, **10**, 7869–7877.
29 I. Roh, S. Yu, C. Lin, S. Louisia, S. Cestellos and P. Yang, *J. Am. Chem. Soc.*, 2022, **144**, 8002–8006.
30 X. Lu, S. Xie, H. Yang, Y. Tong and H. Ji, *Chem. Soc. Rev.*, 2014, **43**, 7581–7593.
31 Z. Zhang and H. Wu, *RSC Adv.*, 2014, **4**, 37395–37399.
32 H. G. Cha and K. S. Choi, *Nat. Chem.*, 2015, **7**, 328–333.
33 J. J. Roylance, T. W. Kim and K. S. Choi, *ACS Catal.*, 2016, **6**, 1840–1847.
34 C. R. Lhermitte and K. Sivula, *ACS Catal.*, 2019, **9**, 2007–2017.
35 S. Li, Z. Li, H. Yu, M. R. Sytu, Y. Wang, D. Beeri, W. Zheng, B. D. Sherman, C. G. Yoo and G. Leem, *ACS Energy Lett.*, 2020, **5**, 777–784.
36 C. R. Lhermitte, N. Plainpan, P. Canjura, F. Boudoirea and K. Sivula, *RSC Adv.*, 2021, **11**, 198–202.
37 Y. Wu, R. Song and J. Li, *Org. Chem. Front.*, 2020, **7**, 1895–1902.
38 M. Zhang, C. Chen, W. Ma and J. Zhao, *Angew. Chem., Int. Ed.*, 2008, **47**, 9730–9733.
39 H. Lu, J. Zhao, L. Li, L. Gong, J. Zheng, L. Zhang, Z. Wang, J. Zhang and Z. Zhu, *Energy Environ. Sci.*, 2011, **4**, 3384–3388.
40 S. Meng, X. Ye, J. Zhang, X. Fu and S. Chen, *J. Catal.*, 2018, **367**, 159–170.
41 J. A. Treadway, J. A. Moss and T. J. Meyer, *Inorg. Chem.*, 1999, **38**, 4386–4387.
42 W. Song, A. K. Vannucci, B. H. Farnum, A. M. Lapides, M. K. Brennaman, B. Kalanyan, L. Alibabaei, J. J. Concepcion, M. D. Losego, G. N. Parsons and T. J. Meyer, *J. Am. Chem. Soc.*, 2014, **136**, 9773–9779.
43 T. V. Pho, M. V. Sheridan, Z. A. Morseth, B. D. Sherman, T. J. Meyer, J. M. Papanikolas, K. S. Schanze and J. R. Reynolds, *ACS Appl. Mater. Interfaces*, 2016, **8**, 9125–9133.
44 L. Bai, F. Li, Y. Wang, H. Li, X. Jiang and L. Sun, *Chem. Commun.*, 2016, **52**, 9711–9714.
45 J. Jiang, B. D. Sherman, Y. Zhao, R. He, I. Ghiviriga, L. Alibabaei, T. J. Meyer, G. Leem and K. S. Schanze, *ACS Appl. Mater. Interfaces*, 2017, **9**, 19529–19534.
46 D. Badgurjar, B. Shan, A. Nayak, L. Wu, R. Chitta and T. J. Meyer, *ACS Appl. Mater. Interfaces*, 2020, **12**, 7768–7776.
47 E. Nikoloudakis, P. B. Pati, G. Charalambidis, D. S. Budkina, S. Diring, A. Planchat, D. Jacquemin, E. Vauthey, A. G. Coutsolelos and F. Odobel, *ACS Catal.*, 2021, **11**, 12075–12086.
48 D. Antón, E. E. Moore, M. A. Bajada, A. Eisenschmidt, A. R. Oliveira, I. A. C. Pereira, J. Warnan and E. Reisner, *Nat. Synth.*, 2022, **1**, 77–86.
49 J. J. Concepcion, J. W. Jurss, M. R. Norris, Z. Chen, J. L. Templeton and T. J. Meyer, *Inorg. Chem.*, 2010, **49**, 1277–1279.
50 S. Yun, N. Vlachopoulos, A. Qurashi, S. Ahmad and A. Hagfeldt, *Chem. Soc. Rev.*, 2019, **48**, 3705–3722.
51 B. Bozic, E. C. Constable and C. E. Housecroft, *Coord. Chem. Rev.*, 2013, **257**, 3089–3106.
52 P. Subramanyam, M. Deepa, S. S. K. Raavi, H. Misawa, V. Biju and C. Subrahmanyam, *Nanoscale Adv.*, 2020, **2**, 5591–5599.
53 H. Tateno, Y. Miseki and K. Sayama, *ChemElectroChem*, 2017, **4**, 3283–3287.
54 R. Zhang, M. Shao, Z. Li, F. Ning, M. Wei, D. G. Evans and X. Duan, *Chem. Eur. J.*, 2017, **23**, 8142–8147.
55 L. Luo, Z. Wang, X. Xiang, D. Yan and J. Ye, *ACS Catal.*, 2020, **10**, 4906–4913.
56 L. Luo, T. Zhang, M. Wang, R. Yun and X. Xiang, *ChemSusChem*, 2020, **13**, 5173–5184.
57 A. W. Harris, O. Yehezkeli, G. R. Hafenstine, A. P. Goodwin and J. N. Cha, *ACS Sustainable Chem. Eng.*, 2017, **5**, 8199–8204.
58 D. Liu, J. Liu, W. Cai, J. Ma, H. B. Yang, H. Xiao, J. Li, Y. Xiong, Y. Huang and B. Liu, *Nat. Commun.*, 2019, 1779.
59 L. Huang, T. Vo and C. Chiang, *Electrochim. Acta*, 2019, **322**, 134725.
60 T. Vo, C. Kao, J. Kuo, C. Chiu and C. Chiang, *Appl. Catal., B*, 2020, **278**, 119303.
61 Y. Wu, D. A. Kuznetsov, N. C. Pflug and C. R. Müller, *J. Mater. Chem. A*, 2021, **9**, 6252–6260.
62 L. Luo, W. Chen, S. Xu, J. Yang, M. Li, H. Zhou, M. Xu, M. Shao, X. Kong, Z. Li and H. Duan, *J. Am. Chem. Soc.*, 2022, **144**, 7720–7730.
63 Y. Liu, M. Wang, B. Zhang, D. Yan and X. Xiang, *ACS Catal.*, 2022, **12**, 6946–6957.
64 H. Tateno, S. Chen, Y. Miseki, T. Nakajima, T. Mochizuki and K. Sayama, *ACS Sustainable Chem. Eng.*, 2022, **10**, 7586–7594.
65 T. Newhouse, P. S. Baran and R. W. Hoffmann, *Chem. Soc. Rev.*, 2009, **38**, 3010–3021.
66 N. Z. Burns, P. S. Baran and R. W. Hoffmann, *Angew. Chem., Int. Ed.*, 2009, **48**, 2854–2867.
67 T. Cernak, K. D. Dykstra, S. Tyagarajan, P. Vachalb and S. W. Krska, *Chem. Soc. Rev.*, 2016, **45**, 546–576.
68 W. R. Gutekunsta and P. S. Bara, *Chem. Soc. Rev.*, 2011, **40**, 1976–1991.

69 M. Zhao and W. Lu, *Org. Lett.*, 2017, **19**, 4560–4563.
70 D. G. Yu, T. Gensch, F. de Azambuja, S. Vasquez and F. Glorius, *J. Am. Chem. Soc.*, 2014, **136**, 17722–17725.
71 X. Yang, Q. Yang, X. Wang, H. Xu, T. Mei, Y. Huang and P. Fang, *J. Org. Chem.*, 2020, **85**, 3497–3507.
72 A. John and K. M. Nicholas, *Organometallics*, 2012, **31**, 7914–7920.
73 Z. Li, L. Luo, M. Li, W. Chen, Y. Liu, J. Yang, S. Xu, H. Zhou, L. Ma, M. Xu, X. Kong and H. Duan, *Nat. Commun.*, 2021, **12**, 6698.
74 K. Ohkubo and K. Hirose, *Angew. Chem., Int. Ed.*, 2018, **57**, 2126–2129.
75 Y. Wang, Q. Yang, P. J. Walsh and E. J. Schelter, *Org. Chem. Front.*, 2022, **9**, 2612–2620.
76 T. Li, T. Kasahara, J. He, K. E. Dettelbach, G. M. Sammis and C. P. Berlinguette, *Nat. Commun.*, 2017, **8**, 390.
77 H. Tateno, S. Iguchi, Y. Miseki and K. Sayama, *Angew. Chem., Int. Ed.*, 2018, **57**, 11238–11241.
78 M. Gong, J. K. Kim, X. Zhao, Y. Li, M. Huang and Y. Wu, *Green Chem.*, 2019, **21**, 3615–3620.
79 J. Ma, K. Mao, J. Low, Z. Wang, D. Xi, W. Zhang, H. Ju, Z. Qi, R. Long, X. Wu, L. Song and Y. Xiong, *Angew. Chem., Int. Ed.*, 2021, **60**, 9357–9361.
80 Y. Jiang, Y. Fan, S. Li and Z. Tang, *CCS Chem.*, 2022, 1–15.
81 R. Hili and A. Yudin, *Nat. Chem. Biol.*, 2006, **2**, 284–287.
82 C. Lamberth, S. Jeanmart and T. Luksch, *Science*, 2013, **341**, 742–746.
83 I. Sorribes, K. Junge and M. Beller, *J. Am. Chem. Soc.*, 2014, **136**, 14314–14319.
84 F. Collet, C. Lescota and P. Dauban, *Chem. Soc. Rev.*, 2011, **40**, 1926–1936.
85 D. Hazelard, P. Nocquet and P. Compain, *Org. Chem. Front.*, 2017, **4**, 2500–2521.
86 H. J. Kim, J. Kim, S. H. Cho and S. Chang, *J. Am. Chem. Soc.*, 2011, **133**, 16382–16385.
87 N. Sauermann, R. Mei and L. Ackermann, *Angew. Chem., Int. Ed.*, 2018, **57**, 5090.
88 T. Morofuji, A. Shimizu and J. Yoshida, *J. Am. Chem. Soc.*, 2013, **135**, 5000–5003.
89 T. Morofuji, A. Shimizu and J. Yoshida, *Chem. Eur. J.*, 2015, **21**, 3211–3214.
90 C. Song, H. Yi, B. Dou, Y. Li, A. K. Singha and A. Lei, *Chem. Commun.*, 2017, **53**, 3689–3692.
91 S. Das, P. Natarajan and B. König, *Chem. Eur. J.*, 2017, **23**, 18161.
92 L. Zhang, L. Liardet, J. Luo, D. Ren, M. Grätzel and X. Hu, *Nat. Catal.*, 2019, **2**, 366–373.
93 H. Fu, P. Tan, R. W. S. Li, H. Liu, Y. Yang and Z. Wu, *J. Hazard. Mater.*, 2022, **424**, 127494.
94 D. Joly, P. A. Bouit and M. Hissler, *J. Mater. Chem. C*, 2016, **4**, 3686–3698.
95 J. Wang, X. Li, J. Li, T. Lei, H. Wu, X. Nan, C. Tung and L. Wu, *Chem. Commun.*, 2019, **55**, 10376–10379.
96 Y. Liu, C. Wang, D. Xue, M. Xiao, C. Li and J. Xiao, *Chem. Eur. J.*, 2017, **23**, 3051.
97 B. Lin, S. Shi, R. Lin, Y. Cui, M. Fang, G. Tang and Y. Zhao, *J. Org. Chem.*, 2018, **83**, 6754–6761.
98 M. Ghobrial, K. Harhammer, M. D. Mihovilovica and M. Schnürch, *Chem. Commun.*, 2010, **46**, 8836–8838.
99 T. Nobuta, N. Tada, A. Fujiya, A. Kariya, T. Miura and A. Itoh, *Org. Lett.*, 2013, **15**, 574–577.
100 Q. Li, X. Zhao, Y. Li, M. Huang, J. K. Kim and Y. Wu, *Org. Biomol. Chem.*, 2017, **15**, 9775–9778.
101 X. Su, F. Yang, Y. Wu and Y. Wu, *Org. Biomol. Chem.*, 2018, **16**, 2753–2756.
102 D. S. Brandes and J. A. Ellman, *Chem. Soc. Rev.*, 2022, **51**, 6738–6756.
103 D. R. Pye and N. P. Mankad, *Chem. Sci.*, 2017, **8**, 1705–1718.
104 M. Gong, M. Huang, Y. Li, J. Zhang, J. K. Kim, J. S. Kim and Y. Wu, *Green Chem.*, 2022, **24**, 837–845.
105 H. Tateno, Y. Miseki and K. Sayama, *Chem. Commun.*, 2017, **53**, 4378–4381.
106 X. Wang, Y. Huang, J. Liao, Z. Wei, W. Li, Y. Xu, H. Chen and D. Kuang, *Nat. Commun.*, 2021, **12**, 1202.
107 H. Rao, W. Li, B. Chen, D. Kuang and C. Su, *Adv. Mater.*, 2017, **29**, 1602639.
108 H. Rao, B. Chen, X. Wang, D. Kuang and C. Su, *Chem. Commun.*, 2017, **53**, 5163–5166.
109 P. Farràs, C. D. Giovanni, J. N. Clifford, E. Palomares and A. Llobet, *Coord. Chem. Rev.*, 2015, **304–305**, 202–208.
110 Y. Zhao, C. Deng, D. Tang, L. Ding, Y. Zhang, H. Sheng, H. Ji, W. Song, W. Ma, C. Chen and J. Zhao, *Nat. Catal.*, 2021, **4**, 684–691.
111 C. Hansch, A. Leo and R. W. Taft, *Chem. Rev.*, 1991, **91**, 165–195.
112 A. Badalyan and S. S. Stahl, *Nature*, 2016, **535**, 406–410.
113 D. S. Choi, H. Lee, F. Tieves, Y. W. Lee, E. J. Son, W. Zhang, B. Shin, F. Hollmann and C. B. Park, *ACS Catal.*, 2019, **9**, 10562–10566.
114 M. Ko, Y. Kim, J. Woo, B. Lee, R. Mehrotra, P. Sharma, J. Kim, S. W. Hwang, H. Y. Jeong, H. Lim, S. H. Joo, J. W. Jang and J. H. Kwak, *Nat. Catal.*, 2022, **5**, 37–44.
115 J. Kim, J. Jang, T. Hilberath, F. Hollmann and C. B. Park, *Nat. Synth.*, 2022, **1**, 776–786.
116 Y. W. Lee, P. Boonmongkolras, E. J. Son, J. Kim, S. H. Lee, S. K. Kuk, J. W. Ko, B. Shin and C. B. Park, *Nat. Commun.*, 2018, **9**, 4208.
117 D. S. Choi, Y. Ni, E. Fernandez, M. Lee, F. Hollmann and C. B. Park, *ACS Catal.*, 2017, **7**, 1563–1567.
118 Y. Chen, T. Lei, H. Hu, H. Wu, S. Zhou, X. Li, B. Chen, C. Tung and L. Wu, *Matter*, 2021, **4**, 2354–2366.
119 C. Ponce de León, *Nat. Catal.*, 2020, **3**, 96–97.
120 X. Shi, S. Back, T. M. Gill, S. Siahrostami and X. Zheng, *Chem*, 2021, **7**, 38–63.
121 I. Schmidt, A. Krogh, K. Wienberg, A. Carlsson, M. Brorson and C. J. H. Jacobsen, *Chem. Commun.*, 2000, **21**, 2157–2158.
122 Z. Song, X. Feng, N. Sheng, D. Lin, Y. Li, Y. Liu, X. Chen, X. Zhou, D. Chen and C. Yang, *Catal. Today*, 2020, **347**, 102–109.
123 J. M. Campos, G. Blanco and J. L. G. Fierro, *Angew. Chem., Int. Ed.*, 2006, **45**, 6962–6984.
124 Y. Wang, D. Lan, R. Durrani and F. Hollmann, *Curr. Opin. Chem. Biol.*, 2017, **37**, 1–9.

125 D. Monti, G. Ottolina, G. Carrea and S. Riva, *Chem. Rev.*, 2011, **111**, 4111–4140.
126 Y. Liang, J. Wei, X. Qiu and N. Jiao, *Chem. Rev.*, 2018, **118**, 4912–4945.
127 W. B. Black, L. Zhang, W. S. Mak, S. Maxel, Y. Cui, E. King, B. Fong, A. S. Martinez, J. B. Siegel and H. Li, *Nat. Chem. Biol.*, 2020, **16**, 87–94.
128 I. Zachos, S. Güner, A. Essert, P. Lommes and V. Sieber, *Chem. Commun.*, 2022, **58**, 11945–11948.